

Discrete-time Integral Resonant Control of Negative Imaginary Systems: Application to a High-speed Nanopositioner

Kanghong Shi, Erfan Khodabakhshi, Prosanto Biswas, Ian R. Petersen, *Life Fellow, IEEE*,
and S. O. Reza Moheimani, *Fellow, IEEE*

Abstract—We propose a discrete-time integral resonant control (IRC) approach for negative imaginary (NI) systems, which overcomes several limitations of continuous-time IRC. We show that a discrete-time IRC has a step-advanced negative imaginary property. A zero-order hold-sampled NI system can be asymptotically stabilized using a discrete-time IRC with suitable parameters. A hardware experiment is conducted where a high-speed flexure-guided nanopositioner is efficiently damped using the proposed discrete-time IRC with the discrete-time controller being implemented in FPGA hardware at the sampling rate of 1.25 MHz.

Index Terms—Integral Resonant Control (IRC), Negative Imaginary (NI) System, Discrete-time System, Digital Control, Nanopositioning.

I. INTRODUCTION

Control design for highly resonant flexible structures poses significant challenges since their structural modes can limit the stability margin and impair the performance of the controlled system [1]–[3]. For instance, in atomic force microscopy (AFM), the resonant mode of the positioner negatively impacts the maximum closed-loop bandwidth, restricting the AFM to only low-speed scanning [2], [4], [5]. Additionally, external disturbances can trigger the resonance, further undermining closed-loop performance [6], [7]. Therefore, it is essential to effectively dampen these resonant modes to simplify the control system design and ensure the closed-loop system’s stability and robustness [3].

Those equipped with collocated actuator-sensor pairs in lightly damped flexible structures can facilitate control design, especially when dealing with plant uncertainties and unmodeled dynamics. [8], [9]. A system with collocated force actuators and position sensors typically has the negative imaginary (NI) property [10], [11]. Based on the NI stability theorem [10], the positive feedback interconnection of an NI plant $G(s)$ and a strictly negative imaginary (SNI) controller $R(s)$ will be internally stable, provided that the largest eigenvalue of the DC loop gain is less than unity; i.e., $\lambda_{\max}(G(0)R(0)) < 1$ [10].

This work was supported by the Australian Research Council under grant DP230102443, and partially by the UTD Center for Atomically Precise Fabrication of Solid-state Quantum Devices.

Kanghong Shi and Ian R. Petersen are with the School of Engineering, College of Engineering, Computing and Cybernetics, Australian National University, Canberra, ACT 2601, Australia. Erfan Khodabakhshi, Prosanto Biswas and S. O. Reza Moheimani are with the Erik Jonsson School of Engineering and Computer Science, The University of Texas at Dallas, Richardson, TX 75080 USA. Corresponding author: S. O. Reza Moheimani. kanghong.shi@anu.edu.au, erfan@utdallas.edu, prosanto.biswas@utdallas.edu, ian.petersen@anu.edu.au, reza.moheimani@utdallas.edu

NI systems theory was introduced in [10], [11] to address the robust control problem for flexible structures [12]–[14]. Several difficulties are associated with the control of flexible structures, such as variable resonance frequencies, high system order, and highly resonant dynamics. These challenges can severely compromise the performance of the control system or cause instability if the controller is not robust against these uncertainties [15]–[18]. NI systems theory offers a framework to evaluate the robustness and design robust controllers for flexible structures in the case of collocated force actuators and position sensors [10], [11], [16].

Roughly speaking, a square, real-rational, proper transfer matrix $G(s)$ is said to be NI if it is stable and for all positive frequencies $\omega > 0$, its frequency response $G(j\omega)$ has negative imaginary parts. An NI system can be regarded as the cascade of a passive system with an integrator. In comparison to passivity theory, which can deal with systems of relative degree zero and one [19], an advantage of NI systems theory is that it can deal with systems of relative degree zero, one and two [20], [21]. Since it was introduced, NI systems theory has attracted attention among control theorists (see e.g., [22]–[28]) and has found its application in many fields including nanopositioning control [29]–[33], the control of lightly damped structures [9], [34], [35], and the control of electrical power systems [36], [37], etc.

Several popular SNI controllers, including the positive position feedback (PPF) controller [38]–[43], the resonant controller (RC) [13], [14], [44], [45], and the integral resonant controller (IRC) [6], [46]–[48], have been implemented successfully. These controllers are not only easy to implement but also highly effective in terms of providing robust damping, especially when dealing with uncertainties in resonance frequency [38]. Among these methods, integral resonant control stands out as a straightforward, low-order approach that can damp multiple modes while maintaining stability margins [3], [17], [38].

The general concept of an integral resonant controller is to modify the pole-zero interlacing of a collocated system $G(s)$ into a zero-pole interlacing pattern by: a) introducing a feed-through term D to the system $G(s)$ and, b) adding an integral controller $C(s) = \Gamma/s$ to the augmented system $\hat{G}(s) = G(s) + D$; see [46], [49]. When the integral gain Γ increases, the system’s poles shift away from the imaginary axis and deeper into the left-half complex plane, finally aligning with the open-loop zero locations. Owing to its straightforward implementation and robust performance, IRC has been widely adopted to enhance damping in a variety of applications, including cantilever beams [46], [50], [51], flexible robotic

manipulators [48], nanopositioning stages [17], atomic force microscopes [52], [53], flexible civil structures [54], [55], and floors subject to vibrations induced by walking [55].

Most literature on nanopositioning focuses on control design within the continuous s -domain rather than the discrete-time z -domain. These control strategies are typically articulated through continuous-time state-space models. For real-time applications, however, it is necessary to discretize these models and solve them in discrete-time steps using a fixed step size. While this discretization process enables the practical application of continuous-time controllers in real-time scenarios, transforming a continuous-time design into a discrete-time implementable version may introduce inaccuracies, particularly for designing damping controllers at higher frequencies. Such a control design method, where a controller is designed based on a continuous-time model and then discretized, is called the continuous-time design or CTD; see [56] and the references therein. A drawback of the CTD technique is its dependency on a sampling rate that is high enough to ensure stability. However, attaining such a high sampling frequency can exceed the capabilities of some devices [57]. Also, as for the digital control of a nanopositioner, the continuous-time model of a nanopositioner is usually estimated via sampled data, which introduces inaccuracies to the control design. To overcome these limitations of a continuous-time IRC, we seek to construct a discrete-time IRC that is designed according to an accurate model of the plant and allows for a relatively slower sampling rate.

In this article, we introduce a discrete-time IRC for the digital control of real-world NI systems. We consider the discrete-time NI system property introduced in [58], where the discrete-time NI property will always be satisfied by a zero-order hold (ZOH) sampled continuous-time NI system (see [59] for a discussion of ZOH sampling). Under some assumptions, a discrete-time NI system can be stabilized using another discrete-time NI system whose output takes a one-step advance, which is called a discrete-time step advanced negative imaginary (SANI) system. We show that a discrete-time IRC is an SANI system. Also, we show that the interconnection of a linear NI system and a discrete-time IRC is asymptotically stable if the IRC parameters satisfy certain conditions related to the DC gain of the plant. Therefore, the digital control problem for an NI system reduces to the process of finding a pair of suitable parameters based on the DC gain of the NI plant. Also, since the NI property is usually guaranteed by a system's physical nature and is preserved under ZOH sampling, the plant's model does not need to be known in the control design process, yet the closed-loop stability is still rigorously guaranteed.

Compared with the continuous-time IRC, the advantages of using a discrete-time IRC are two-fold: a) The controller design process is more straightforward as we do not need to reconstruct a continuous-time model of the plant and discretize the controller. This significantly saves the computational resources required in generating the control input; b) Stability is rigorously guaranteed and less reliant on a high sampling rate since the stability analysis is carried out purely in discrete time without any type of approximation.

When implementing a discrete-time controller, selecting an appropriate step size is crucial to maintain stability. If the step size is too large, the solver may become unstable, necessitating a reduction in step size. However, there is a practical lower limit on how small the step size can be, especially when the controller runs on hardware with limited computational capabilities. The processing unit requires adequate time to execute necessary calculations at each step. For instance, controlling a system with a high mechanical bandwidth demands a high control loop bandwidth, requiring a smaller step size to ensure accurate implementation. If the step size is inadequate, the controller might not function as intended, compromising system performance. Therefore, ensuring that the processing speed is sufficient to handle the controller's computational complexity within the bandwidth of the system is vital.

The discrete-time IRC is designed and implemented for a high-speed, high-bandwidth nanopositioning system. The controller implementation was performed using a LabVIEW program and a National Instruments PXIe-7975R FlexRIO module. A NI-5782 adapter module with a 250 MHz clock speed was used to acquire the digital data and implement the discrete-time IRC at a sampling rate of 1.25 MHz.

The rest of this article is organized as follows: Section II provides preliminary results on continuous-time IRC and also discrete-time NI systems theory. In Section III, we introduce the discrete-time IRC. To be specific, we provide the system model of a discrete-time IRC and show that it is an SANI system. We also prove that the interconnection of a discrete-time NI system and a discrete-time IRC is asymptotically stable under some conditions on the IRC parameters. In Section IV, a hardware experiment is conducted where a discrete-time IRC is applied to a high-speed flexure-guided nanopositioner. We conclude the article in Section V.

Notation: The notation in this paper is standard. \mathbb{R} denotes the field of real numbers. \mathbb{N} denotes the set of nonnegative integers. $\mathbb{R}^{m \times n}$ denotes the space of real matrices of dimension $m \times n$. A^T denotes the transpose of a matrix A . A^{-T} denotes the transpose of the inverse of A ; that is, $A^{-T} = (A^{-1})^T = (A^T)^{-1}$. $\lambda_{max}(A)$ denotes the largest eigenvalue of a matrix A with real spectrum. $\|\cdot\|$ denotes the standard Euclidean norm. For a real symmetric or complex Hermitian matrix P , $P > 0$ ($P \geq 0$) denotes the positive (semi-)definiteness of a matrix P and $P < 0$ ($P \leq 0$) denotes the negative (semi-)definiteness of a matrix P . A function $V : \mathbb{R}^n \rightarrow \mathbb{R}$ is said to be positive definite if $V(0) = 0$ and $V(x) > 0$ for all $x \neq 0$.

II. PRELIMINARIES

A. Continuous-time integral resonant controller

Integral resonant control (IRC) was introduced in [46], [50] to provide damping for flexible structures with collocated and compatible actuator/sensor pairs (e.g. force actuators and position sensors). Fig. 1 shows how a continuous-time IRC is implemented. Given a plant with a square transfer matrix $G(s)$, we apply a direct feedthrough D and also an integral controller

$$C(s) = \frac{\Gamma}{s} \quad (1)$$

in positive feedback with $G(s) + D$. Here, we require the matrices $\Gamma, D \in \mathbb{R}^{p \times p}$ to satisfy $D < 0$ and $\Gamma > 0$. The relation between the plant input $U(s)$ and the plant output $Y(s)$ is described as follows:

$$U(s) = C(s)e(s) = C(s)(r + Y(s) + DU(s)). \quad (2)$$

Hence,

$$U(s) = (I - C(s)D)^{-1}C(s)(r + Y(s)). \quad (3)$$

According to (3), the closed-loop system shown in Fig. 1 can be equivalently constructed as the interconnection of $G(s)$ and $K(s)$ shown in Fig. 2, where

$$K(s) := (I - C(s)D)^{-1}C(s). \quad (4)$$

Substituting (1) into (4) yields

$$K(s) := (sI - \Gamma D)^{-1}\Gamma. \quad (5)$$

Here, $K(s)$ given in (5) is the transfer matrix of a continuous-time IRC. An IRC is an SNI system, and can be used in the control of NI plants (see [10], [11], [50]).

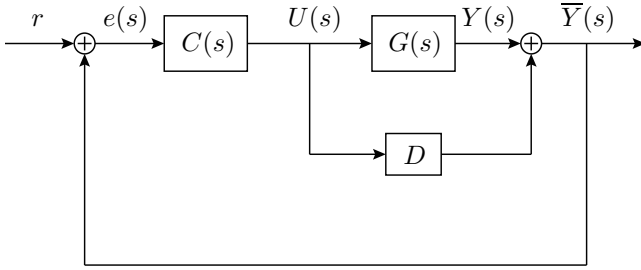


Fig. 1. Closed-loop interconnection of an integrator $C(s) = \frac{\Gamma}{s}$ and $G(s) + D$.

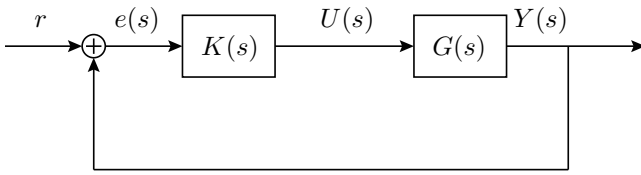


Fig. 2. Closed-loop interconnection of an IRC and a plant. This is equivalent to the closed-loop system in Fig. 1.

B. Discrete-time NI systems

We consider the definition of discrete-time NI systems introduced in [58]. This property is automatically satisfied by any ZOH sampled continuous-time NI system. A discrete-time NI system can be stabilized by another discrete-time NI system with a step advance. First, we provide the definition of discrete-time NI systems given in [58].

Consider the system

$$x_{k+1} = f(x_k, u_k), \quad (6a)$$

$$y_k = h(x_k), \quad (6b)$$

where $f : \mathbb{R}^n \times \mathbb{R}^p \rightarrow \mathbb{R}^n$ and $h : \mathbb{R}^n \rightarrow \mathbb{R}^p$. Here $u_k, y_k \in \mathbb{R}^p$ and $x_k \in \mathbb{R}^n$ are the input, output and state of the system at time step $k \in \mathbb{N}$, respectively.

Definition 1 (discrete-time negative imaginary systems): [58] The system (6) is said to be a discrete-time negative imaginary (NI) system if there exists a continuous positive definite function $V : \mathbb{R}^n \rightarrow \mathbb{R}$ such that for arbitrary x_k and u_k ,

$$V(x_{k+1}) - V(x_k) \leq u_k^T (y_{k+1} - y_k), \quad (7)$$

for all k .

In the case of a linear system, necessary and sufficient conditions are given under which the system satisfies Definition 1. Consider a linear system of the form

$$\Sigma: x_{k+1} = Ax_k + Bu_k, \quad (8a)$$

$$y_k = Cx_k, \quad (8b)$$

where $x_k \in \mathbb{R}^n$, $u_k, y_k \in \mathbb{R}^p$ are the system state, input and output, respectively. Here $A \in \mathbb{R}^{n \times n}$, $B \in \mathbb{R}^{n \times p}$ and $C \in \mathbb{R}^{p \times n}$.

Lemma 1: [58] Suppose the linear system (8) satisfies $\det(I - A) \neq 0$. Then the system (8) is NI with a quadratic positive definite storage function satisfying (7) if and only if there exists a real matrix $P = P^T > 0$ such that

$$A^T P A - P \leq 0 \quad \text{and} \quad C = B^T (I - A)^{-T} P. \quad (9)$$

A discrete-time NI system can be stabilized using a discrete-time step advanced NI (SANI) system. An SANI system can be obtained by replacing the output of an NI system using the output at the next time step. We provide the definition of SANI systems in the following. Consider the system

$$\tilde{x}_{k+1} = \tilde{f}(\tilde{x}_k, \tilde{u}_k), \quad (10a)$$

$$\tilde{y}_k = \tilde{h}(\tilde{x}_k, \tilde{u}_k), \quad (10b)$$

where $\tilde{f} : \mathbb{R}^n \times \mathbb{R}^p \rightarrow \mathbb{R}^n$ and $\tilde{h} : \mathbb{R}^n \rightarrow \mathbb{R}^p$. Here $\tilde{u}, \tilde{y} \in \mathbb{R}^p$ and $\tilde{x} \in \mathbb{R}^n$ are the input, output and state of the system at time step $k \in \mathbb{N}$, respectively.

Definition 2: [58] The system (10) is said to be a step-advanced negative imaginary (SANI) system if there exists a function $\hat{h}(x_k)$ such that:

- 1) $\tilde{h}(\tilde{x}_k, \tilde{u}_k) = \hat{h}(\tilde{f}(\tilde{x}_k, \tilde{u}_k))$;
- 2) There exists a continuous positive definite function $\tilde{V} : \mathbb{R}^n \rightarrow \mathbb{R}$ such that for arbitrary state \tilde{x}_k and input \tilde{u}_k ,

$$\tilde{V}(\tilde{x}_{k+1}) - \tilde{V}(\tilde{x}_k) \leq \tilde{u}_k^T \left(\hat{h}(\tilde{x}_{k+1}) - \hat{h}(\tilde{x}_k) \right)$$

for all k .

Remark 1: Definition 2 can be regarded as a variant of Definition 1 in a way such that the system output y_k takes the next step output value; i.e., $h(x_{k+1})$. To be specific, suppose the system (6) is NI as per Definition 1. Then a system with the same state equation (6a) and an output equation $\tilde{y}(k) = h(x(k+1)) = h(f(x_k, u_k))$ is a SANI system. Note that this does not affect the causality of the system because $h(f(x_k, u_k))$ is a function of the state x_k and input u_k of the current step k .

III. DISCRETE-TIME INTEGRAL RESONANT CONTROLLER

Since real-world control systems are usually implemented digitally using computers [59], we aim to find the discrete-time version of the IRC in order to provide digital control for NI plants. Considering that sampling a continuous-time NI plant yields a discrete-time NI system, a discrete-time IRC is required to serve as a controller for a discrete-time NI system.

As is mentioned in Section II-B, a discrete-time NI system can be stabilized using a discrete-time SANI system. A continuous-time NI system $K(s)$, which has SNI property, is expected to become a discrete-time NI system after ZOH sampling. Therefore, taking a step advance of a ZOH sampled IRC will result in an SANI system. However, a disadvantage of taking the ZOH discretization of $K(s)$ is that the model of the resulting system will include matrix exponential terms. In order to achieve a neat system model for the discrete-time IRC, we first construct a discrete-time system of the similar form as $K(s)$ in (4), except that the continuous-time integrator $C(s)$ is replaced by a discrete-time integrator

$$C(z) = \frac{\Gamma}{z-1}. \quad (11)$$

This discrete-time system has the transfer matrix

$$\begin{aligned} K(z) &= (I - C(z)D)^{-1} C(z) \\ &= \left(I - \frac{\Gamma D}{z-1} \right) \frac{\Gamma}{z-1} \\ &= [zI - (I + \Gamma D)]^{-1} \Gamma. \end{aligned} \quad (12)$$

We still require that $\Gamma > 0$ and $D < 0$. However, the matrices Γ and D here are not related to those in the continuous-time IRC. A state-space realization of the transfer matrix $K(z)$ is given as follows:

$$\tilde{x}_{k+1} = (I + \Gamma D)\tilde{x}_k + \Gamma\tilde{u}_k, \quad (13a)$$

$$\hat{y}_k = \tilde{x}_k, \quad (13b)$$

where $\tilde{x}_k, \tilde{u}_k, \hat{y}_k \in \mathbb{R}^p$ are system state, input and output, respectively. We show in the following that the system (13) is a discrete-time NI system when certain conditions are satisfied for the matrices Γ and D .

Lemma 2: Suppose $\Gamma > 0$ and $-2\Gamma^{-1} \leq D < 0$, then the system (13) with the transfer matrix $K(z)$ is a discrete-time NI system.

Proof: We apply Lemma 1 to show the NI property of (13). Let

$$\bar{A} = (I + \Gamma D), \quad (14)$$

$$\bar{B} = \Gamma, \quad (15)$$

$$\bar{C} = I. \quad (16)$$

Then $\det(I - \bar{A}) = \det(-\Gamma D) \neq 0$. We show in the following that the matrix $\bar{P} = -D$ satisfies the conditions in (9). We have

$$\begin{aligned} \bar{A}^T \bar{P} A - \bar{P} &= -D - 2D\Gamma D - D\Gamma D\Gamma D + D \\ &= -2D\Gamma D - D\Gamma D\Gamma D \\ &= -D\Gamma(2\Gamma^{-1} + D)\Gamma D \\ &\leq 0. \end{aligned} \quad (17)$$

Also, we have

$$\bar{B}^T (I - \bar{A})^{-T} \bar{P} = \Gamma(-\Gamma D)^{-T}(-D) = I = \bar{C}. \quad (18)$$

Therefore, the system (13) with the transfer matrix $K(z)$ in (12) is NI. ■

We have shown that the system (13), which is constructed in a similar way as the continuous-time IRC, is a discrete-time NI system. However, according to the control framework for discrete-time NI systems in [58], an NI system can be applied as the controller for another NI system after introducing one step advance in its output equation. Therefore, we introduce one step advance to the output of the system (13), which yields the following system.

$$\tilde{x}_{k+1} = (I + \Gamma D)\tilde{x}_k + \Gamma\tilde{u}_k, \quad (19a)$$

$$\tilde{y}_k = (I + \Gamma D)\tilde{x}_k + \Gamma\tilde{u}_k, \quad (19b)$$

where $\tilde{x}_k, \tilde{u}_k, \hat{y}_k \in \mathbb{R}^p$ are system state, input and output, respectively. Here, $\Gamma > 0$ and $-2\Gamma^{-1} \leq D < 0$. The transfer matrix of the system (19) is

$$F(z) = z[zI - (I + \Gamma D)]^{-1} \Gamma. \quad (20)$$

We call the system (19) the discrete-time integral resonant controller. Since the system is obtained by taking one step advance of the NI system (13), it is an SANI system and hence we expect the interconnection of a linear NI plant with the system (19) to be at least Lyapunov stable. We provide a particular stability proof in the following and show that asymptotic stability can indeed be achieved for the interconnection of an NI plant and a discrete-time IRC of the form (19). First, we prove the SANI property of the discrete-time IRC (19).

Lemma 3: Suppose $\Gamma > 0$ and $-2\Gamma^{-1} \leq D < 0$. Then the discrete-time integral resonant controller (19) is an SANI system.

Proof: The proof follows directly from Definitions 1 and 2 and Lemma 2. To be specific, since the system (19) is obtained by taking one step advance of the NI system (13), then the function $\hat{h}(x_k) = x_k$ satisfies Condition 1) in Definition 2 and Condition 2) is satisfied due to the NI property of the system (13) as shown in Lemma 2. ■

Now consider a linear discrete-time system with the minimal realization

$$x_{k+1} = Ax_k + Bu_k, \quad (21a)$$

$$y_k = Cx_k, \quad (21b)$$

where $x_k \in \mathbb{R}^n$, $u_k, y_k \in \mathbb{R}^p$ are the system state, input and output, respectively. Here, $A \in \mathbb{R}^{n \times n}$, $B \in \mathbb{R}^{n \times p}$ and $C \in \mathbb{R}^{p \times n}$. The transfer matrix of the system (21) is

$$G(z) = C(zI - A)^{-1}B. \quad (22)$$

We show in the following that if the system (21) is NI, then

there exists a discrete-time IRC of the form (19) such that their closed-loop interconnection is asymptotically stable.

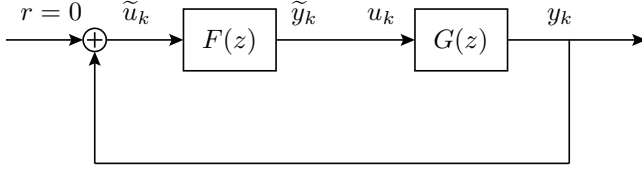


Fig. 3. Positive feedback interconnection of the plant $G(z)$ of the form (21) and a discrete-time IRC $F(z)$ of the form (19).

Theorem 1: Consider the closed-loop interconnection of the minimal system (21) and a discrete-time IRC of the form (19), as is shown in Fig. 3. Suppose the system (21) with the transfer matrix $G(z)$ satisfies $\det(I - A) \neq 0$ and is an NI system according to Definition 1. If the discrete-time IRC (19) satisfies $-2\Gamma^{-1} < D < -G(1)$, then the closed-loop system shown in Fig. 3 is asymptotically stable.

Proof: According to Lemma 1, the NI property of the plant (21) implies that there exists a symmetric positive definite matrix $P \in \mathbb{R}^{n \times n}$ such that

$$A^T P A - P \leq 0; \quad (23)$$

$$C = B^T (I - A)^{-T} P. \quad (24)$$

According to the system setting $\tilde{u}_k = y_k$ and $u_k = \tilde{y}_k$ as shown in Fig. 3, we have

$$\begin{aligned} x_{k+1} &= Ax_k + Bu_k \\ &= Ax_k + B\tilde{y}_k \\ &= Ax_k + B[(I + \Gamma D)\tilde{x}_k + \Gamma\tilde{u}_k] \\ &= Ax_k + B[(I + \Gamma D)\tilde{x}_k + \Gamma y_k] \\ &= Ax_k + B[(I + \Gamma D)\tilde{x}_k + \Gamma C x_k] \\ &= (A + B\Gamma C)x_k + B(I + \Gamma D)\tilde{x}_k, \end{aligned} \quad (25)$$

and

$$\begin{aligned} \tilde{x}_{k+1} &= (I + \Gamma D)\tilde{x}_k + \Gamma\tilde{u}_k \\ &= (I + \Gamma D)\tilde{x}_k + \Gamma y_k \\ &= (I + \Gamma D)\tilde{x}_k + \Gamma C x_k, \end{aligned} \quad (26)$$

where the equalities also use (19) and (21). Therefore, according to (25) and (26), the closed-loop system shown in Fig. 3 has the state-space model

$$\begin{bmatrix} x_{k+1} \\ \tilde{x}_{k+1} \end{bmatrix} = \begin{bmatrix} A + B\Gamma C & B + B\Gamma D \\ \Gamma C & I + \Gamma D \end{bmatrix} \begin{bmatrix} x_k \\ \tilde{x}_k \end{bmatrix}. \quad (27)$$

Let

$$\hat{A} := \begin{bmatrix} A + B\Gamma C & B + B\Gamma D \\ \Gamma C & I + \Gamma D \end{bmatrix}. \quad (28)$$

In what follows, we apply Lyapunov's stability theorem. We construct the candidate Lyapunov function of the closed-loop system in Fig. 3 to be:

$$W(x_k, x_{k+1}) = \frac{1}{2} \begin{bmatrix} x_k \\ \tilde{x}_k \end{bmatrix}^T \begin{bmatrix} P & -C^T \\ -C & -D \end{bmatrix} \begin{bmatrix} x_k \\ \tilde{x}_k \end{bmatrix}, \quad (29)$$

where P is the positive definite matrix that satisfies (23) and

(24). Let

$$Q := \begin{bmatrix} P & -C^T \\ -C & -D \end{bmatrix}. \quad (30)$$

We prove in the following that $Q > 0$. The condition (24) implies

$$B = (I - A)P^{-1}C^T. \quad (31)$$

Using (31), we have that

$$G(1) = C(I - A)^{-1}B = CP^{-1}C^T > 0. \quad (32)$$

Since $P > 0$ and the Schur complement of the block P of the matrix Q is

$$Q/P = -D - CP^{-1}C^T = -D - G(1), \quad (33)$$

which is positive definite according to the assumption on D , then we have $Q > 0$. Since $Q > 0$ and $D < 0$, we also have that

$$Q/(-D) = P + C^T D C > 0. \quad (34)$$

Now we take the increment of the candidate Lyapunov function $W(x_k, \tilde{x}_k)$ to show stability. We have

$$\begin{aligned} W(x_{k+1}, \tilde{x}_{k+1}) - W(x_k, \tilde{x}_k) \\ = \frac{1}{2} \begin{bmatrix} x_k \\ \tilde{x}_k \end{bmatrix}^T (\hat{A}^T Q \hat{A} - Q) \begin{bmatrix} x_k \\ \tilde{x}_k \end{bmatrix}. \end{aligned} \quad (35)$$

Using (31), we have that

$$\hat{A}^T Q \hat{A} - Q = \begin{bmatrix} M_{11} & M_{12} \\ M_{12}^T & M_{22} \end{bmatrix}, \quad (36)$$

where

$$\begin{aligned} M_{11} &= (C^T \Gamma C P^{-1} - I) (A^T P A - P) (I - P^{-1} C^T \Gamma C) \\ &\quad - 2C^T \Gamma C - C^T \Gamma D \Gamma C; \end{aligned} \quad (37)$$

$$\begin{aligned} M_{12} &= (C^T \Gamma C P^{-1} - I) (A^T P A - P) P^{-1} C^T (I + \Gamma D) \\ &\quad - C^T \Gamma D (2I + \Gamma D); \end{aligned} \quad (38)$$

$$\begin{aligned} M_{22} &= (I + D\Gamma) C P^{-1} (A^T P A - P) P^{-1} C^T (I + \Gamma D) \\ &\quad - D\Gamma D \Gamma D - 2D\Gamma D. \end{aligned} \quad (39)$$

According to (37)–(39), we have that

$$\begin{aligned} \hat{A}^T Q \hat{A} - Q \\ = \begin{bmatrix} C^T \Gamma C - P \\ (I + D\Gamma) C \end{bmatrix} P^{-1} (A^T P A - P) P^{-1} \begin{bmatrix} C^T \Gamma C - P \\ (I + D\Gamma) C \end{bmatrix}^T \\ - \begin{bmatrix} C^T \Gamma \\ D\Gamma \end{bmatrix} (D + 2\Gamma^{-1}) \begin{bmatrix} C^T \Gamma \\ D\Gamma \end{bmatrix}^T. \end{aligned} \quad (40)$$

Here, we have $A^T P A - P \leq 0$ according to (23) and $D + 2\Gamma^{-1} > 0$ according to the assumption of the theorem. Therefore, both terms on the right-hand side (RHS) of (40) are negative semidefinite. Hence, the matrix $\hat{A}^T Q \hat{A} - Q$ is negative semidefinite. This implies that $W(x_{k+1}, \tilde{x}_{k+1}) - W(x_k, \tilde{x}_k) \leq 0$. That is, the closed-loop system shown in Fig. 3 is stable in the sense of Lyapunov. We will show in the following that the closed-loop system is asymptotically stable using LaSalle's invariance principle (see e.g., [60], [61]). According to (35) and (40), if $W(x_{k+1}, \tilde{x}_{k+1}) - W(x_k, \tilde{x}_k)$ stays at zero, then the scalar

$$\begin{bmatrix} x_k \\ \tilde{x}_k \end{bmatrix}^T \begin{bmatrix} C^T \Gamma \\ D \Gamma \end{bmatrix} (D + 2\Gamma^{-1}) \begin{bmatrix} C^T \Gamma \\ D \Gamma \end{bmatrix}^T \begin{bmatrix} x_k \\ \tilde{x}_k \end{bmatrix} \quad (41)$$

also stays at zero. This is because both terms on the RHS of (40) are negative semidefinite and can only contribute non-positive values to $W(x_{k+1}, \tilde{x}_{k+1}) - W(x_k, \tilde{x}_k)$. If (41) stays at zero, then since $(D + 2\Gamma^{-1}) > 0$ and $\Gamma > 0$, it follows that

$$\begin{bmatrix} C & D \end{bmatrix} \begin{bmatrix} x_k \\ \tilde{x}_k \end{bmatrix} \quad (42)$$

stays at zero. That is $Cx_k + D\tilde{x}_k \equiv 0$. In this case,

$$\tilde{x}_k \equiv -D^{-1}Cx_k. \quad (43)$$

Substituting (43) in (26), we have

$$\tilde{x}_{k+1} \equiv \tilde{x}_k \quad (44)$$

Since $\det D \neq 0$, then (43) and (44) together imply that for all future time steps k

$$Cx_k \equiv \alpha, \quad (45)$$

for some constant vector α . According to the observability of the system (21), (45) implies

$$x_{k+1} \equiv x_k. \quad (46)$$

Substituting (43) in (25), we have

$$x_{k+1} \equiv (A - BD^{-1}C)x_k. \quad (47)$$

Using (31), we have that

$$\begin{aligned} A - BD^{-1}C &= A - (I - A)P^{-1}C^T D^{-1}C \\ &= (A - I)P^{-1}(P + C^T DC) + I. \end{aligned} \quad (48)$$

We have $\det(A - I) \neq 0$ according to the assumption of the theorem and also $\det(P + C^T DC) \neq 0$ according to (34). Therefore,

$$(A - I)P^{-1}(P + C^T DC)x_k \neq 0 \quad (49)$$

for any nonzero x_k . Substituting (48) in (47) with (49) also considered, we have that

$$x_{k+1} \neq x_k \quad (50)$$

unless $x_k = 0$. In the case that $x_k = 0$, we also have $\tilde{x}_k = 0$ according to (43). Hence, the system state already stays at the equilibrium at the origin. Otherwise, $W(x_{k+1}, \tilde{x}_{k+1}) - W(x_k, \tilde{x}_k)$ cannot stay at zero. Therefore, $W(x_k, \tilde{x}_k)$ will keep decreasing until it reaches zero. That is, the system state also reaches the origin. Therefore, the closed-loop interconnection shown in Fig. 3 is asymptotically stable. ■

Remark 2: The condition $-2\Gamma^{-1} < D < -G(1)$ of the IRC parameters can be fulfilled in two steps. Given the matrix $G(1)$, we choose D such that $D < -G(1)$. Then we choose Γ such that $\Gamma < -2D^{-1}$. Note that since $G(1) > 0$ according to (32), then for matrices Γ and D that satisfy $-2\Gamma^{-1} < D < -G(1)$, they also satisfy the conditions in Lemma 3.

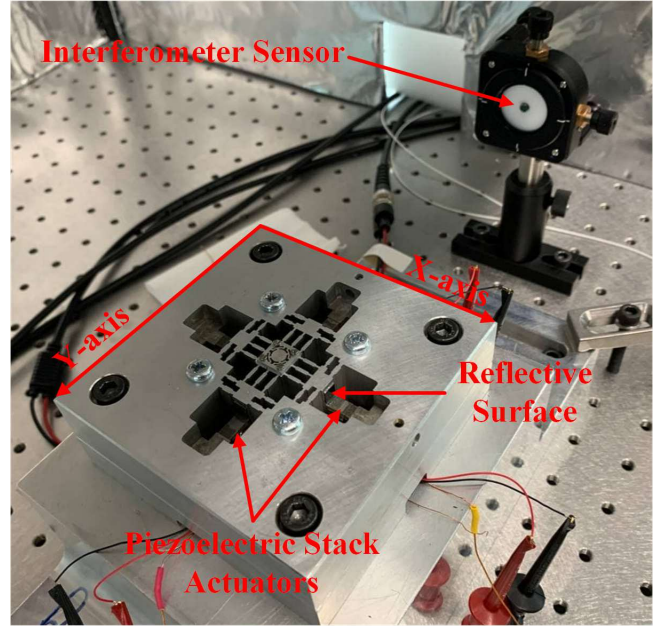


Fig. 4. Nanopositioner and interferometer sensor

IV. HIGH-SPEED FLEXURE-GUIDED NANOPositionER

In this section, a discrete-time IRC is designed and implemented on a high-speed flexure-guided nanopositioner as a linear NI system to demonstrate the applicability of the stability result.

Figure 4 demonstrates the experimental setup of a high-speed flexure-guided nanopositioner introduced in [62]. The nanopositioning stage is driven by four PiezoDrive PX200 voltage amplifiers (each with a gain of 20) for all piezoelectric actuators. A PICOSCALE interferometer is used for high-precision displacement measurements of the nanopositioner in both X - and Y -directions. Under ideal conditions, the lightly-damped nanopositioner with collocated actuators and sensors would be an NI system. However, due to the fabrication tolerances and bandwidth limitations of the driving electronics, the nanopositioner violates the NI system property beyond a certain frequency where the phase surpasses -180° . Figure 5 shows the frequency response function (FRF) of the X -axis nanopositioner from actuation to the sensor output. The fundamental resonance frequency of the nanopositioner along X -axis is at 14.86 kHz. We see that the phase drops beyond 15.01 kHz, and the system violates the NI property as frequency increases. However, as the frequency response rolls off, the phase deviation is negligible. Therefore, the frequency response of the system can be approximated by a NI model within the frequency range of interest. The implementation of the designed IRC is described in the next sections.

A. Experimental Setup

Figure (6) shows a schematic representation of the experimental apparatus. A high-precision Michelson-interferometer is employed to measure the displacement of the scanner. The measurement from the optical sensor is transmitted as Digital

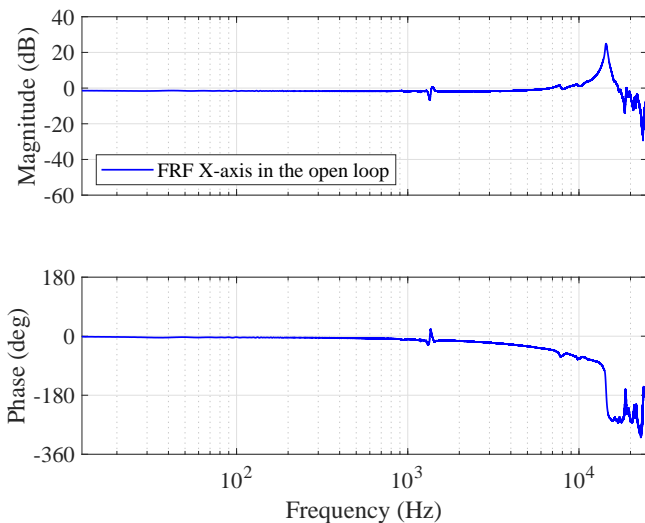


Fig. 5. Frequency response of the nanopositioner.

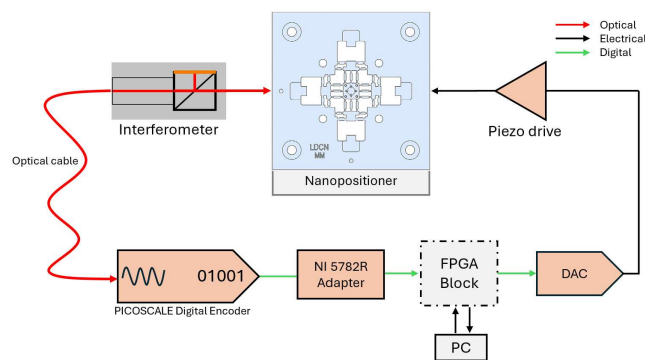


Fig. 6. A schematic of the experimental apparatus.

Differential Interface (DDI) outputs via the PICO SCALE Breakout Box (BOB). These DDI outputs configured as a Quadrature (AquadB) signal from the BOB are then carefully adjusted for the desired resolution within our implementable bandwidth in the form of step size and step frequency. Subsequently, we implement a standard quadrature decoder within the LabVIEW FPGA environment to derive position values in μm alongside the designed discrete-time integral resonant controller.

The operating principle of the quadrature decoder is as follows: it utilizes two phases of the encoder, Quad A and Quad B, which are spaced at 90-degree intervals. This arrangement allows the logic operations to determine the direction of movement. The decoder uses the current state of B and the previous state of A to obtain the direction of movement and adjust the counting value accordingly, either adding or subtracting one count from the previous value. Since PICO SCALE only measures relative position changes, an initialization process is necessary for accurate counting, facilitated by a reset circuit. Subsequently, each count is multiplied by a position scaling factor determined from the step size. Through experimentation, it is found that the sensor noise is slightly below 6 nm, leading to the configuration of

the sensor step size to be precisely 6 nm for each count. Figure 7 illustrates an excerpt of the implemented quadrature decoder in the LabVIEW environment, responsible for converting DDI output into position parameters.

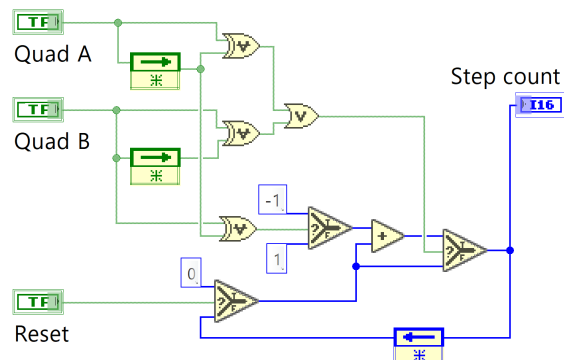


Fig. 7. Quadrature decoder implemented in LabVIEW FPGA.

B. FPGA Implementation

In this experiment, a Kintex-7 XC7K410T FPGA embedded in a National Instruments PXIe-7975R FlexRIO module is adopted as the core computing engine. This module interfaces with an adapter module, offering hardware description language integration capability. The FPGA hardware is developed using the graphical programming language in the LabVIEW FPGA environment. Connected to the FlexRIO module is the National Instruments 5782R adapter module, a 14-bit, four-channel digitizer with a bandwidth of 500 MHz and a sampling rate of 250 MS/s. Each component is programmed within a single-cycled timed loop (SCTL) to optimize hardware design performance and minimize computational latency. This loop ensures specific timing cycles for executing one iteration, provided there is no timing violation during compilation. Additionally, a voltage converter is employed to adjust the DDI output level from the BOB to match the adapter's input voltage level. With its high sampling rate of 250 MHz, the decoder swiftly transforms digital data into position parameters. However, the involvement of multiplications in our first-order discrete-time IRC within each loop, spanning multiple

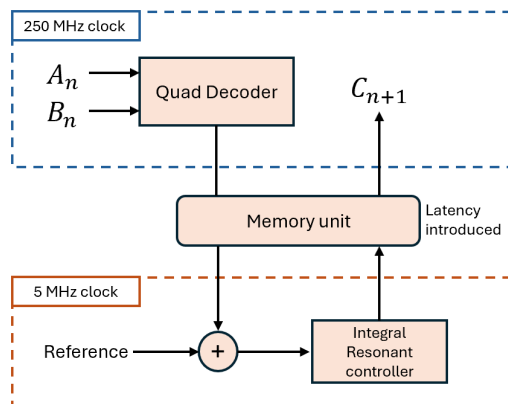


Fig. 8. Parallel computation inside FPGA.

clock cycles, surpasses the 4 ns time limit. As a result, the decoded position data is transmitted to a slower SCTL, which operates at a clock frequency of 5 MHz. This frequency is derived from the primary oscillator of 250 MHz, as illustrated in figure (8). This additional data transfer latency, coupled with register usage between loops, further reduces the achievable sampling rate to 1.25 MHz, necessitating the implementation of the discrete-time IRC at this reduced rate.

When dealing with a high clock frequency, computational speed becomes an issue. Integer-type variables are favored due to their faster processing, resulting in shorter computation times, especially in the high-frequency loop. Conversely, in the slower loop, fixed-point data formats are employed for variables and parameters, offering the advantage of customizable range and resolution for calculations. Comparatively, the discrete-time design of the IRC proves computationally more efficient than its continuous-time counterpart. Observations indicate that the discrete-time IRC requires less memory and computational resources for its implementation within the same data format, thus minimizing the latency.

C. Discrete-time IRC Design

According to Theorem 1, the closed-loop interconnection of the minimal system (21) and a discrete-time IRC of the form (19) is asymptotically stable if the discrete-time IRC (19) satisfies $-2\Gamma^{-1} < D < -G(1)$. Controller parameters can be tuned to achieve the desired performance in the time and frequency domain. Accordingly, $D = -3$ and $\Gamma = 0.010$ are opted for in the discrete-time IRC.

The frequency response of the nanopositioner in a closed loop with the discrete-time IRC is depicted in Fig.9. We observe that a substantial damping of about 14.4 dB is achieved at the resonance.

We also applied a unity step as an input disturbance to the system and analyzed the damped system response in a closed loop. Figure 10 demonstrates the step response of the flexure-guided nanopositioner in an open loop and closed loop with the discrete-time IRC in a positive feedback interconnection.

V. CONCLUSION

In this article, we introduce the discrete-time IRC to provide efficient and rigorous digital control for NI systems. We show that a discrete-time IRC has SANI property. With suitable parameters chosen, a discrete-time IRC can asymptotically stabilize an NI system. This stability result motivates the application of the discrete-time IRC on a high-speed flexure-guided nanopositioner. It is shown in a hardware experiment that a nanopositioner can be effectively damped by a discrete-time IRC.

REFERENCES

- [1] H. Pota, S. O. R. Moheimani, and M. Smith, "Resonant controllers for flexible structures," in *Proceedings of the 38th IEEE Conference on Decision and Control (Cat. No. 99CH36304)*, vol. 1. IEEE, 1999, pp. 631–636.
- [2] S. Devasia, E. Eleftheriou, and S. O. R. Moheimani, "A survey of control issues in nanopositioning," *IEEE Transactions on Control Systems Technology*, vol. 15, no. 5, pp. 802–823, 2007.

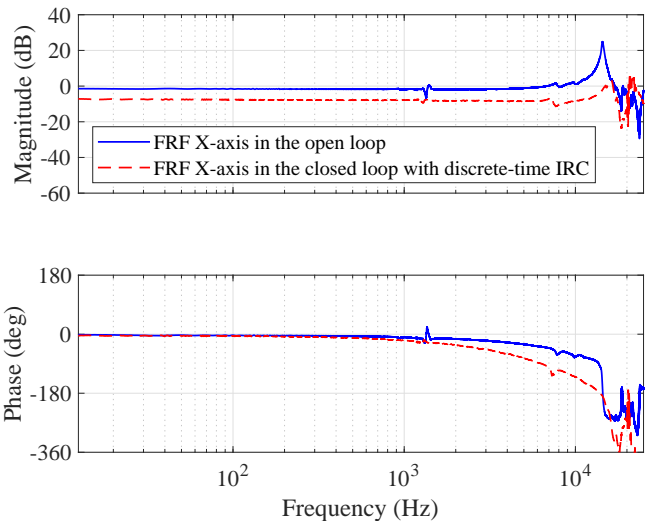


Fig. 9. Bode plot of the flexure-guided nanopositioner in open loop and in a positive feedback interconnection with the discrete-time IRC.

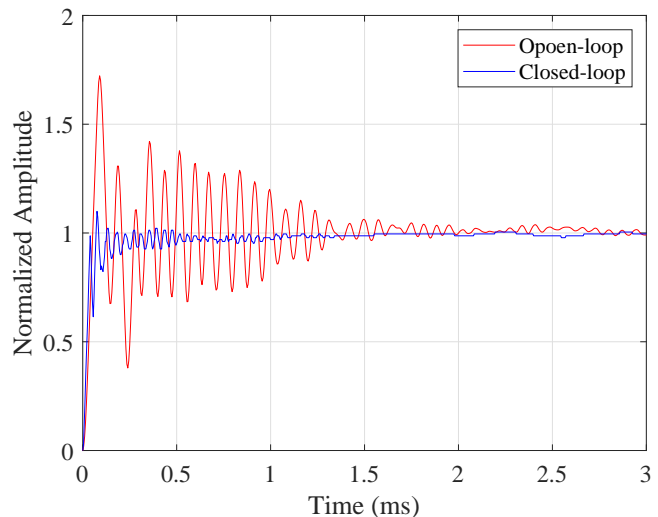


Fig. 10. Normalized Step Response of the flexure-guided nanopositioner in open loop and damped closed-loop.

- [3] N. Nikoienjad and S. O. R. Moheimani, "Frequency domain-based integral resonant control design for a MEMS nanopositioner," in *2021 IEEE Conference on Control Technology and Applications (CCTA)*. IEEE, 2021, pp. 874–879.
- [4] S. O. R. Moheimani, "Invited review article: Accurate and fast nanopositioning with piezoelectric tube scanners: Emerging trends and future challenges," *Review of Scientific Instruments*, vol. 79, no. 7, 2008.
- [5] H. Habibullah, H. R. Pota, and I. Petersen, "A robust control approach for high-speed nanopositioning applications," *Sensors and Actuators A: Physical*, vol. 292, pp. 137–148, 2019.
- [6] A. J. Fleming, S. S. Aphale, and S. O. R. Moheimani, "A new method for robust damping and tracking control of scanning probe microscope positioning stages," *IEEE Transactions on nanotechnology*, vol. 9, no. 4, pp. 438–448, 2009.
- [7] A. A. Eielson, M. Vagia, J. T. Gravdahl, and K. Y. Pettersen, "Damping and tracking control schemes for nanopositioning," *IEEE/ASME Transactions on Mechatronics*, vol. 19, no. 2, pp. 432–444, 2013.
- [8] I. R. Petersen, "Negative imaginary systems theory in the robust control of highly resonant flexible structures," in *2011 Australian Control Conference*. IEEE, 2011, pp. 1–6.
- [9] B. Bhikkaji, S. O. R. Moheimani, and I. R. Petersen, "A negative imaginary approach to modeling and control of a collocated structure," *IEEE/ASME Transactions on Mechatronics*, vol. 17, no. 4, pp. 717–727, 2012.

- 2011.
- [10] A. Lanzon and I. R. Petersen, "Stability robustness of a feedback interconnection of systems with negative imaginary frequency response," *IEEE Transactions on Automatic Control*, vol. 53, no. 4, pp. 1042–1046, 2008.
 - [11] I. R. Petersen and A. Lanzon, "Feedback control of negative-imaginary systems," *IEEE Control Systems Magazine*, vol. 30, no. 5, pp. 54–72, 2010.
 - [12] A. Preumont, *Vibration control of active structures: an introduction*. Springer, 2018, vol. 246.
 - [13] D. Halim and S. O. R. Moheimani, "Spatial resonant control of flexible structures-application to a piezoelectric laminate beam," *IEEE Transactions on Control Systems Technology*, vol. 9, no. 1, pp. 37–53, 2001.
 - [14] H. Pota, S. O. R. Moheimani, and M. Smith, "Resonant controllers for smart structures," *Smart Materials and Structures*, vol. 11, no. 1, p. 1, 2002.
 - [15] E. Omid and N. Mahmoodi, "Hybrid positive feedback control for active vibration attenuation of flexible structures," *IEEE/ASME Transactions on Mechatronics*, vol. 20, no. 4, pp. 1790–1797, 2014.
 - [16] I. R. Petersen, "Negative imaginary systems theory and applications," *Annual Reviews in Control*, vol. 42, pp. 309–318, 2016.
 - [17] E. Khodabakhshi, N. Nikooinnejad, M. Maroufi, and S. O. R. Moheimani, "Characterization and control of a piezoelectrically actuated high-speed planar nanopositioner," in *2022 IEEE Conference on Control Technology and Applications (CCTA)*. IEEE, 2022, pp. 1313–1318.
 - [18] H. Feng, H. Zhou, C. Jiang, and A. Pang, "High precision structured h-infinity control of a piezoelectric nanopositioning platform," *Plos one*, vol. 18, no. 6, p. e0286471, 2023.
 - [19] B. Brogliato, R. Lozano, B. Maschke, and O. Egeland, *Dissipative systems analysis and control: theory and applications*. Springer, London, 2007, vol. 2.
 - [20] K. Shi, I. R. Petersen, and I. G. Vladimirov, "Necessary and sufficient conditions for state feedback equivalence to negative imaginary systems," *IEEE Transactions on Automatic Control (Early Access)*, 2024.
 - [21] J. Dannatt and I. R. Petersen, "Strictly negative imaginary state feedback control for relative degree two systems," *arXiv preprint arXiv:2304.01687*, 2023.
 - [22] J. Xiong, I. R. Petersen, and A. Lanzon, "A negative imaginary lemma and the stability of interconnections of linear negative imaginary systems," *IEEE Transactions on Automatic Control*, vol. 55, no. 10, pp. 2342–2347, 2010.
 - [23] M. A. Mabrok, A. G. Kallapur, I. R. Petersen, and A. Lanzon, "Generalizing negative imaginary systems theory to include free body dynamics: Control of highly resonant structures with free body motion," *IEEE Transactions on Automatic Control*, vol. 59, no. 10, pp. 2692–2707, 2014.
 - [24] J. Wang, A. Lanzon, and I. R. Petersen, "Robust cooperative control of multiple heterogeneous negative-imaginary systems," *Automatica*, vol. 61, pp. 64–72, 2015.
 - [25] A. G. Ghallab, M. A. Mabrok, and I. R. Petersen, "Extending negative imaginary systems theory to nonlinear systems," in *2018 IEEE Conference on Decision and Control (CDC)*. IEEE, 2018, pp. 2348–2353.
 - [26] K. Shi, I. R. Petersen, and I. G. Vladimirov, "Output feedback consensus for networked heterogeneous nonlinear negative-imaginary systems with free-body motion," *IEEE Transactions on Automatic Control*, vol. 68, no. 9, pp. 5536–5543, 2023.
 - [27] P. Bhowmick and S. Patra, "On LTI output strictly negative-imaginary systems," *Systems & Control Letters*, vol. 100, pp. 32–42, 2017.
 - [28] M. Mabrok, A. G. Kallapur, I. R. Petersen, and A. Lanzon, "A generalized negative imaginary lemma and Riccati-based static state-feedback negative imaginary synthesis," *Systems & Control Letters*, vol. 77, pp. 63–68, 2015.
 - [29] M. A. Mabrok, A. G. Kallapur, I. R. Petersen, and A. Lanzon, "Spectral conditions for negative imaginary systems with applications to nanopositioning," *IEEE/ASME Transactions on Mechatronics*, vol. 19, no. 3, pp. 895–903, 2013.
 - [30] S. K. Das, H. R. Pota, and I. R. Petersen, "A MIMO double resonant controller design for nanopositioners," *IEEE Transactions on Nanotechnology*, vol. 14, no. 2, pp. 224–237, 2014.
 - [31] —, "Multivariable negative-imaginary controller design for damping and cross coupling reduction of nanopositioners: a reference model matching approach," *IEEE/ASME Transactions on Mechatronics*, vol. 20, no. 6, pp. 3123–3134, 2015.
 - [32] K. Shi, N. Nikooinnejad, I. R. Petersen, and S. O. R. Moheimani, "Negative imaginary control using hybrid integrator-gain systems: Application to MEMS nanopositioner," *IEEE Transactions on Control Systems Technology (Early Access)*, 2023.
 - [33] N. Nikooinnejad and S. O. R. Moheimani, "Convex synthesis of sni controllers based on frequency-domain data: MemS nanopositioner example," *IEEE Transactions on Control Systems Technology*, vol. 30, no. 2, pp. 767–778, 2021.
 - [34] C. Cai and G. Hagen, "Stability analysis for a string of coupled stable subsystems with negative imaginary frequency response," *IEEE Transactions on Automatic Control*, vol. 55, no. 8, pp. 1958–1963, 2010.
 - [35] M. A. Rahman, A. Al Mamun, K. Yao, and S. K. Das, "Design and implementation of feedback resonance compensator in hard disk drive servo system: A mixed passivity, negative-imaginary and small-gain approach in discrete time," *Journal of Control, Automation and Electrical Systems*, vol. 26, no. 4, pp. 390–402, 2015.
 - [36] Y. Chen, I. R. Petersen, and E. L. Ratnam, "Design and stability of angle based feedback control in power systems: A negative-imaginary approach," *To appear in 2024 American Control Conference*, preprint available as *arXiv:2310.01781*, 2023.
 - [37] Y. Chen, K. Shi, I. R. Petersen, and E. L. Ratnam, "A nonlinear negative imaginary systems framework with actuator saturation for control of electrical power systems," *To appear in 2024 European Control Conference*, preprint available as *arXiv:2311.06820*, 2023.
 - [38] D. Russell and S. S. Aphale, "Evaluating the performance of robust controllers for a nanopositioning platform under loading," *IFAC-PapersOnLine*, vol. 50, no. 1, pp. 10895–10900, 2017.
 - [39] C. J. Goh and T. K. Caughey, "On the stability problem caused by finite actuator dynamics in the collocated control of large space structures," *International Journal of Control*, vol. 41, no. 3, pp. 787–802, 1985.
 - [40] J. L. Fanson and T. K. Caughey, "Positive position feedback-control for large space structures," *AIAA Journal*, vol. 28, no. 4, pp. 717–724, April 1990.
 - [41] M. Ratnam, B. Bhikkaji, A. J. Fleming, and S. O. R. Moheimani, "Ppf control of a piezoelectric tube scanner," in *Proc. IEEE CDC-ECC*, December 2005.
 - [42] S. O. R. Moheimani, B. J. G. Vautier, and B. Bhikkaji, "Experimental implementation of extended multivariable PPF control on an active structure," *IEEE Transactions on Control Systems Technology*, vol. 14, no. 3, pp. 443–445, May 2006.
 - [43] M. W. Fairbairn, P. Muller, and S. O. R. Moheimani, "Sensorless implementation of a ppf controller for active q control of an afm microcantilever," *IEEE Transactions on Control Systems Technology*, vol. 22, no. 6, pp. 2118–2126, November 2014.
 - [44] B. J. G. Vautier and S. O. R. Moheimani, "Charge-driven piezoelectric actuators for structural vibration control: Issues and implementation," *Smart Material and Structures*, vol. 14, no. 4, pp. 575–586, 2005.
 - [45] A. Sebastian, A. Pantazi, S. O. R. Moheimani, H. Pozidis, and E. Eleftheriou, "Achieving sub-nanometer precision in a mems storage device during self-servo write process," *IEEE Transactions on Nanotechnology*, vol. 7, no. 5, pp. 586–595, September 2008, digital Object Identifier 10.1109/TNANO.2008.926441.
 - [46] S. S. Aphale, A. J. Fleming, and S. O. R. Moheimani, "Integral resonant control of collocated smart structures," *Smart materials and structures*, vol. 16, no. 2, p. 439, 2007.
 - [47] B. Bhikkaji and S. O. R. Moheimani, "Integral resonant control of a piezoelectric tube actuator for fast nano-scale positioning," *IEEE/ASME Transactions on Mechatronics*, vol. 13, no. 5, pp. 530–537, October 2008.
 - [48] E. Pereira, S. S. Aphale, V. Feliu, and S. O. R. Moheimani, "Integral resonant control for vibration damping and precise tip-positioning of a single-link flexible manipulator," *IEEE/ASME Transactions on Mechatronics*, vol. 16, no. 2, pp. 232–240, 2010.
 - [49] Y. K. Yong, S. S. Aphale, and S. O. R. Moheimani, "Design, analysis and control of a fast nanopositioning stage," in *2008 IEEE/ASME International Conference on Advanced Intelligent Mechatronics*. IEEE, 2008, pp. 451–456.
 - [50] B. Bhikkaji, S. O. R. Moheimani, and I. R. Petersen, "Multivariable integral control of resonant structures," in *2008 47th IEEE Conference on Decision and Control*. IEEE, 2008, pp. 3743–3748.
 - [51] J. D. MacLean and S. S. Aphale, "A modified linear integral resonant controller for suppressing jump-phenomenon and hysteresis in microcantilever beam structures," *Journal of Sound and Vibration*, vol. 480, p. 115365, 2020.
 - [52] S. P. Wadikhaye, Y. K. Yong, B. Bhikkaji, and S. R. Moheimani, "Control of a piezoelectrically actuated high-speed serial-kinematic afm nanopositioner," *Smart materials and structures*, vol. 23, no. 2, p. 025030, 2014.
 - [53] Y. K. Yong and S. R. Moheimani, "Collocated z-axis control of a high-speed nanopositioner for video-rate atomic force microscopy," *IEEE Transactions on Nanotechnology*, vol. 14, no. 2, pp. 338–345, 2015.

- [54] B. Basu and S. R. Nielsen, "A multi-modal control using a hybrid pole-placement-integral resonant controller (ppir) with experimental investigations," *Structural Control and Health Monitoring*, vol. 18, no. 2, pp. 191–206, 2011.
- [55] S. Beskhyroun, L. Wegner, and B. Sparling, "Integral resonant control scheme for cancelling human-induced vibrations in light-weight pedestrian structures, struct. control heal. monit.(2011) n/an."
- [56] D. Nešić, A. R. Teel, and P. V. Kokotović, "Sufficient conditions for stabilization of sampled-data nonlinear systems via discrete-time approximations," *Systems & Control Letters*, vol. 38, no. 4-5, pp. 259–270, 1999.
- [57] D. H. Owens, Y. Zheng, and S. A. Billings, "Fast sampling and stability of nonlinear sampled-data systems: Part 1. existence theorems," *IMA Journal of Mathematical Control and Information*, vol. 7, no. 1, pp. 1–11, 1990.
- [58] K. Shi, I. R. Petersen, and I. G. Vladimirov, "Discrete-time negative imaginary systems from ZOH sampling," *To appear in the proceedings of the 26th International Symposium on Mathematical Theory of Networks and Systems*, preprint available as [arXiv:2312.05419](https://arxiv.org/abs/2312.05419), 2023.
- [59] K. J. Åström and B. Wittenmark, *Computer-controlled systems: theory and design*. Courier Corporation, 2013.
- [60] W. M. Haddad and V. Chellaboina, *Nonlinear dynamical systems and control: a Lyapunov-based approach*. Princeton University Press, 2008.
- [61] W. Mei and F. Bullo, "Lasalle invariance principle for discrete-time dynamical systems: A concise and self-contained tutorial," *arXiv preprint arXiv:1710.03710*, 2017.
- [62] E. Khodabakhshi, N. Nikooienejad, M. Maroufi, and S. O. R. Moheimani, "Design and characterization of a novel high-bandwidth flexure-guided xy nanopositioner," *IFAC-PapersOnLine*, vol. 55, no. 27, pp. 271–276, 2022.